NASA Technical Memorandum 102504

Finite Element Analysis of Thermal Distortion Effects on Optical Performance of Solar Dynamic Concentrator for Space Station *Freedom*

Michael P. Doherty and Vithal Dalsania
Lewis Research Center
Cleveland, Ohio

July 1990

NASA

ENTER:
4B - EM3287.PRT

DISPLAY 03/6/1
91N12954*# ISSUE 4 PAGE 532 CATEGORY 37 RPT#: NASA-TM-102504
E-5305 NAS 1.15:102504 90/07/00 18 PAGES UNCLASSIFIED DOCUMENT
UTTL: Finite element analysis of thermal distortion effects on optical performance of solar dynamic concentrator for Space Station Freedom
AUTH: A/DOHERTY, MICHAEL P.; B/DALSANIA, VITHAL
CORP: National Aeronautics and Space Administration. Lewis Research Center, Cleveland, OH.
SAP: Avail: NTIS HC/MF A03; 3 functional color pages
CIO: UNITED STATES Original contains color illustrations
MAJS: /*CONCENTRATORS/*DISTORTION/*FINITE ELEMENT METHOD/*MATHEMATICAL MODELS/* TEMPERATURE DISTRIBUTION/*TEMPERATURE EFFECTS
MINS: / DISPLACEMENT/ EARTH ORBITS/ RECEIVERS/ SPACE STATION POWER SUPPLIES/ SPACE STATIONS
ABA: Author

Finite Element Analysis of Thermal Distortion Effects on Optical Performance of Solar Dynamic Concentrator for Space Station *Freedom*

Michael P. Doherty and Vithal Dalsania
National Aeronautics and Space Administration
Lewis Research Center
Cleveland, Ohio 44135

Summary

An analysis has been performed to predict the thermal distortion of the solar dynamic concentrator for Space Station *Freedom* in low Earth orbit and to evaluate the effects of that thermal distortion on concentrator on-orbit performance. The analysis required substructural finite element modeling of critical concentrator structural subsystems, structural finite element modeling of the concentrator, mapping of thermal loading onto the structural finite element model, and the creation of specialized postprocessors to assist in interpreting results. Concentrator temperature distributions and thermally induced displacements and slope errors and the resulting receiver flux distribution profiles are discussed. Results determined for a typical orbit indicate that concentrator facet rotations are less than 0.2 mrad and that the change in facet radius due to thermal flattening is less than 5 percent. The predicted power loss due to thermal distortion effects is less than 0.3 percent. As a consequence the thermal distortions of the solar dynamic concentrator in low Earth orbit will have a negligible effect on the flux distribution profiles within the receiver.

Introduction

To generate power for Space Station *Freedom*, NASA will use both photovoltaic and solar dynamic power-generating systems. Four photovoltaic modules will provide 75 kWe (kilowatts of electrical power) for the phase 1 Space Station *Freedom*. Twenty-five-kWe solar dynamic modules are being developed to provide additional power for future growth. The solar dynamic power-generating system is more than four times more efficient in converting thermal energy to electric power than the photovoltaic system. The closed Brayton cycle solar dynamic system collects solar energy to heat a working fluid, which in turn drives a turbine to rotate an electrical generator. A thermal energy storage medium is required to heat the working fluid during the 28- to 36-min eclipse portion of the 95-min orbit.

To collect and focus sunlight for a 25-kWe solar dynamic module, NASA will develop a large solar concentrator that will provide a distributed solar flux within a heat receiver cavity. Since reflective surfaces of this size have not been developed or flown in space, there is a need to predict the optical performance of such large, lightweight solar concentrators. In order to achieve appropriate flux distribution within the heat receiver cavity, concentrator mirrored-surface accuracy and pointing accuracy tolerances are tightly controlled. Identified error sources that will influence the optical performance of the concentrator while it is on orbit include facet alignment in a l-g environment, facet manufacturing errors including slope error and specular reflectance, receiver-to-concentrator alignment, and thermal distortion. In order to maintain its optical performance over a 10-year lifetime, the concentrator must be durable enough to withstand the harsh environment of Space Station *Freedom's* low Earth orbit (LEO). The LEO environment causes degradation of optical and structural surfaces due to atomic oxygen, ultraviolet (UV) radiation, micrometeoroid impacts, and a considerable number of thermal cycles.

This report discusses the analytical determination of solar dynamic concentrator thermal distortion and its effects on concentrator on-orbit optical performance. First, the concentrator is briefly described to establish a familiarity with its geometry. Then, the details of the analysis are presented. Specifically discussed herein are substructural finite element analyses conducted to study concentrator component structural behavior, the creation of a finite element structural model of the concentrator based on findings from the substructural analyses, the development of a specialized analytical procedure for determining thermal distortion and its effects on concentrator optical performance, and the execution of the concentrator analysis. Finally, the results of the structural analysis (the thermal distortion) and the effects of thermal distortion on concentrator on-orbit optical performance are presented and discussed.

Concentrator Description

The concentrator is one of the eight major assemblies of Space Station *Freedom's* solar dynamic module, as shown in figure 1. The concentrator is subdivided into 19 hexagonal panels (hexpanels) sized to fit in the space shuttle's payload bay. The concentrator is an offset parabolic configuration in which the flat hexpanels are fastened together by latches so that each latch point lies on the paraboloid. The primary advantages of the offset parabolic and hexpanel design concepts are the low mass moment of inertia of the solar dynamic module about Space Station *Freedom's* transverse boom and the compactness of the stowed module, which allows for

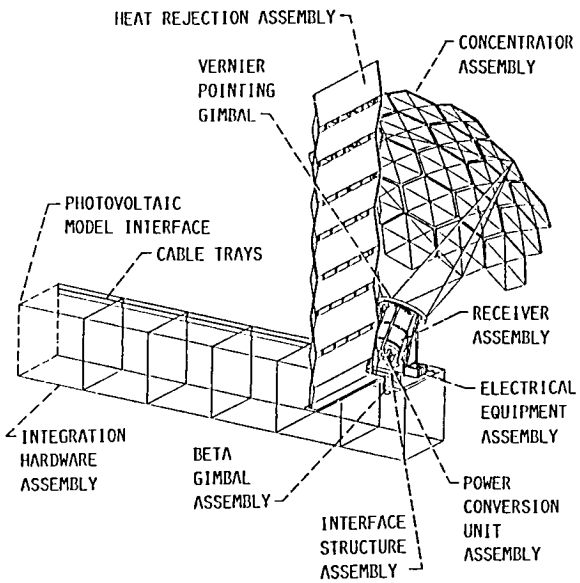

FIGURE 1. - SOLAR DYNAMIC MODULE.

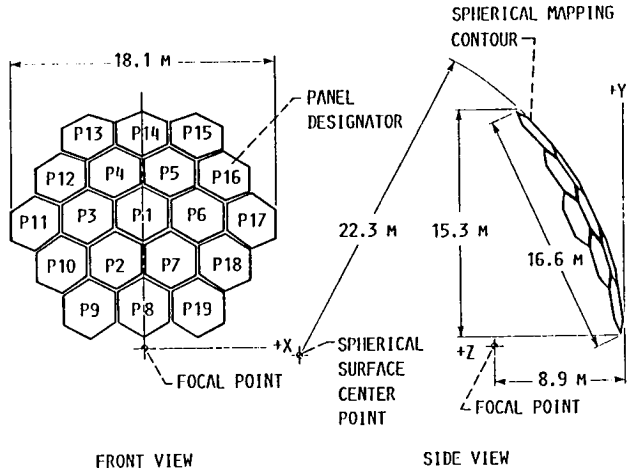

FIGURE 2. - CONFIGURATION OF ADVANCED DEVELOPMENT CONCENTRATOR.

packaging two complete modules in the shuttle payload bay. The concentrator reflective surface area comprises 456 facets, 24 facets per hexpanel. The hexpanels are supported by a nine-strut support structure. Three of the struts provide stiffness to the hexpanels, and the other six struts attach the concentrator assembly to the receiver interface ring at three points. The receiver is tilted approximately 51° with respect to the boresight axis of the Sun to improve the circumferential flux distribution on the heat receiver cavity wall. The thermal design strategy for the concentrator includes using low-absorbance and low-emittance surface coatings to control component temperatures and selecting materials with a very low coefficient of thermal expansion to reduce thermal distortions.

Because the solar dynamic concentrator has not yet been developed, the concentrator analyzed for this report was not the flight concentrator but rather the advanced-development concentrator designed and developed by the Harris Corporation, Government Aerospace Systems Division (ref. 1). NASA contracted with Harris to develop and demonstrate the most effective means of collecting and focusing solar energy to be used in a power-generating system for Space Station *Freedom*. The advanced-development concentrator assembly is mapped to a spherical surface rather than to the ideal parabolic surface. The spherical surface shown in figure 2 allows the hexpanels to be equally spaced on a sphere. Note that the projected views shown in figure 2 distort the appearance of the equally spaced panels. The equal spacing of the hexpanels reduced fabrication costs by decreasing the number of unique latch configurations and drawings.

The details of a hexpanel are shown in figure 3. A hexpanel comprises twelve rectangular-cross-section, graphite-fiber-reinforced epoxy (GFRE) box beams. The 2-m (6.56-ft) long box beams are joined and bonded together at the hub and six corner points by shear plates and corner fitting assemblies.

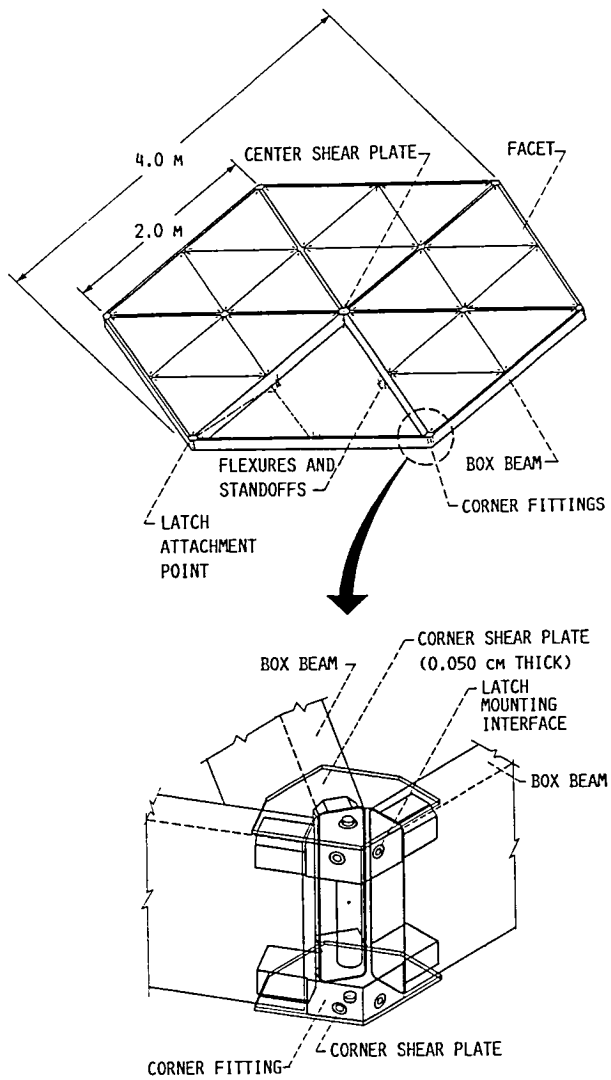

TYPICAL HEXAGONAL CORNERS WHERE THREE BOX BEAMS ARE BONDED TO CORNER FITTINGS AND SHEAR PLATES

FIGURE 3. - DETAILS OF HEXAGONAL PANEL.

The GFRE box beams have a high stiffness-to-weight ratio, a high strength-to-weight ratio, and a very low coefficient of thermal expansion (-0.9×10^6 cm/cm °C). The top and bottom GFRE shear plates provide the load path between the box beams at the six corners and the hub. The aluminum corner fittings define the hexpanel geometry and provide the attachment point for the aluminum latches (ref. 2)

A typical aluminum latch-striker assembly is shown in figure 4. The latch-striker assembly is a self-locking "ball and socket" connector comprising a striker assembly (housing and ball) that fits into a latch assembly (housing, spring-loaded pawl, and striker plate). The striker ball is locked into place with the spring-loaded pawl of the latch assembly. This design provides zero translational displacement in three axes.

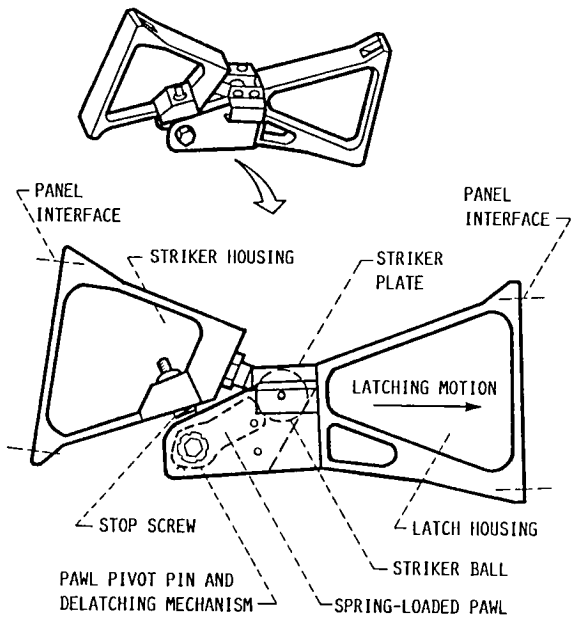

FIGURE 4. - LATCH-STRIKER ASSEMBLY.

In order to concentrate the Sun's rays into the heat receiver, 24 mirrored triangular facets are mounted to each hexpanel with 72 (three each) standoff-flexure assemblies. The standoff-flexure assemblies isolate the facets from loads imposed by boxbeam distortions and allow individual facets to be aligned so that solar flux will be properly distributed within the heat receiver cavity. In order to adequately support the facets, the standoff-flexure assemblies are located both at the ends (near the corner and hub fittings) and at the midspans of the box beams. The details and dimensions of a typical corner-located standoff-flexure assembly are shown in figure 5. The facets have varying spherical radii of curvature and are tilted within the hexpanel frames depending on their specific location on the concentrator. The triangular facets for the advanced-development concentrator measure approximately 1 m on a side and have surface contour radii of 1921, 2181, 2441, or 2702 cm (756.25, 858.75, 961.25, or 1063.75 in.). Four radii facets instead of 456 unique radii facets were chosen for the advanced-development concentrator in spite of a slight increase in slope error because of the large decrease in facet manufacturing (tooling) costs. As shown in figure 6, each facet is made of two 7.5-mil GFRE facesheets bonded to a 0.635-cm (0.25-in.) thick aluminum honeycomb core. The vapor-deposited reflective and protective surfaces consist of aluminum with a magnesium fluoride or silicon oxide coating. Aluminum, although less reflective, was selected over silver for the advanced-development concentrator because of its durability in the terrestrial environment. The specular surface for the reflective coating is provided by an epoxy-rich layer of graphite vail on the facesheet and a polished-surface caul plate (ref. 3).

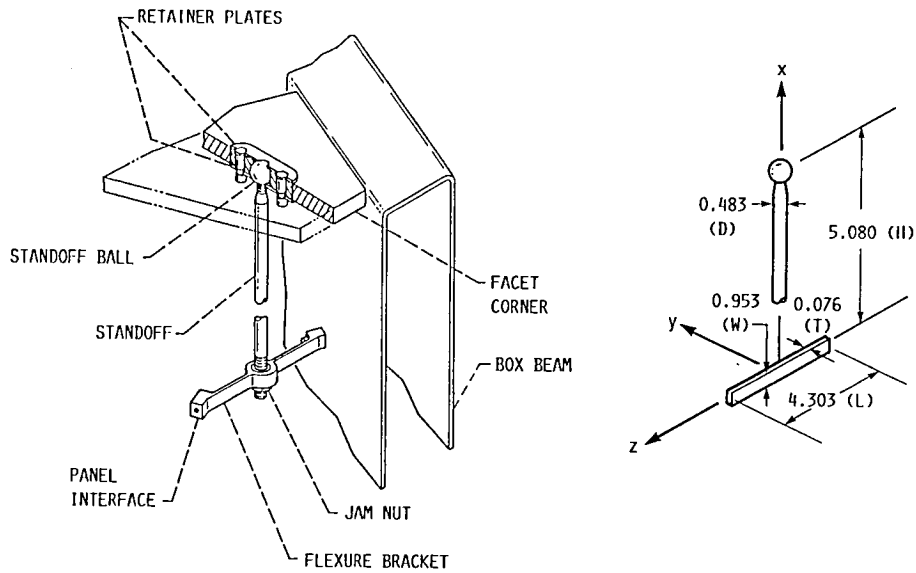

FIGURE 5. - DETAIL AND DIMENSIONS OF STANDOFF-FLEXURE ASSEMBLIES. (DIMENSIONS ARE IN CENTIMETERS.)

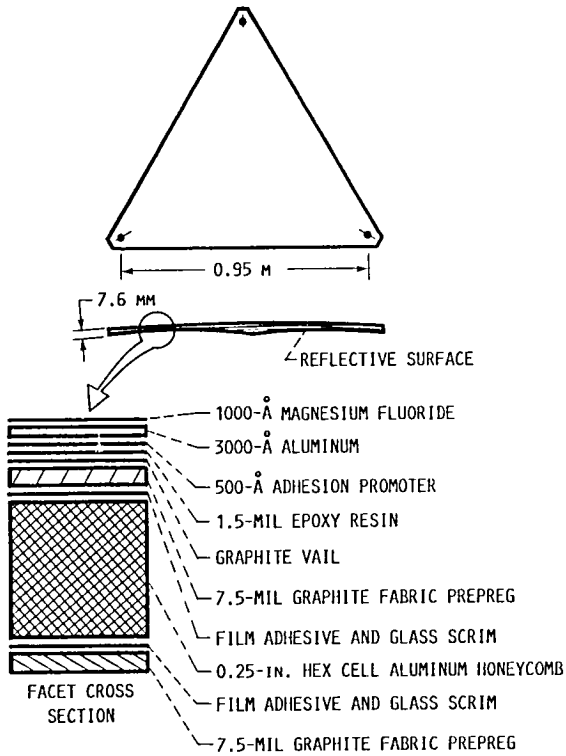

FIGURE 6. - FACET DETAILS.

Thermal Distortion Analysis

The analysis to determine thermal distortion and how it affects concentrator performance consisted of four parts: substructural finite element modeling of distinctive concentrator components, creation of a concentrator finite element model, development of a specialized analytical procedure for determining thermal distortion and its effects, and execution of the concentrator analysis. The concentrator components modeled and analyzed as distinct substructures were a single triangular facet and an entire hexpanel. The findings from these detailed component analyses resulted in a simplified concentrator model. The creation of a finite element model of the concentrator required remodeling a single hexpanel with simplifications, reproducing the hexpanel at 19 separate locations, and adding the remaining necessary modeling detail. A specialized analytical procedure for determining thermal distortion and its effects was needed because the analysis had unique pre- and postprocessing requirements. Computer programs had to be developed at the Lewis Research Center to meet these requirements. These in-house programs, in addition to two commercially available programs, PATRAN (ref. 4) and MSC/NASTRAN (ref. 5), were the basis of the analytical procedure for determining thermal distortion and its effects. (PATRAN is a pre- and postprocessor for interactive creation of finite element models and graphical evaluation of finite element analysis results; MSC/NASTRAN is a general-purpose computer code for structural analysis by the finite element method.) Execution of the concentrator analysis involved running NASTRAN and performing the postprocessing.

The four parts of the analysis are described in detail in the following sections.

Substructural Analysis

The concentrator has two distinct components: the facet and the hexpanel. These two components were modeled in detail to study the effects of thermal loads. Analysis of these substructures was necessary to establish the degree of modeling detail required to accurately predict the thermal distortion of the concentrator. These models were created and analyzed by using PATRAN and NASTRAN. The following paragraphs describe the models and the results of the substructural analyses.

Facet model.—The facet model consisted of one facet and three standoff-flexure assemblies. The facet chosen for substructural analysis was assumed to be supported by three midbeam-located standoff-flexure assemblies, a support configuration representative of one-quarter of the facets making up the concentrator. The other facet support configuration, two midbeam-located standoff-flexure assemblies and one corner-located assembly, was not modeled because of the similarity in the standoff-flexure assemblies between two designs. The model was used to study the effects of uniform temperature rise and linear through-thickness temperature gradient on the single facet and the standoff-flexure assembly. The model was also used to investigate the influence of facet curvature on structural stiffness. In addition, the facet was modeled with two different mesh densities so that the effects of mesh density on the accuracy of the results could be predicted.

The finite element model of a single triangular facet is shown in figure 7. The composite facet structure was initially modeled as being flat and comprising 105 NASTRAN TRIA3 plate elements. Seven bar elements were needed to model each of the midbeam-located standoff-flexure assemblies. The facet facesheet-honeycomb structure was modeled as a sandwich plate. Its membrane and bending behavior were described by quasi-isotropic material elastic constants (GFRE facesheets), and its transverse shear behavior was described by isotropic material elastic constants (honeycomb core). Boundary conditions were established by assuming the points where the flexure assemblies attached to the hexpanel beams to be fixed. A temperature of 73 °C (163 °F) was applied to the standoffs in the form of TEMP cards, and the results were compared with cases where the standoffs were left at room temperature, 21 °C (70 °F). A temperature gradient of 2.2 deg C/cm (10 deg F/in.) from the hotter concave side to the colder convex side was applied to the facet with a TEMPPI card in order to investigate facet-flattening behavior. Then, the facet was remodeled with a coarse 10-element mesh and the results were compared with the results obtained with fine 105-element mesh. Finally, the facet was remodeled to have spherical curvature, using a fine 105-element mesh density.

The results and conclusions of the substructural analysis of the facet were as follows:

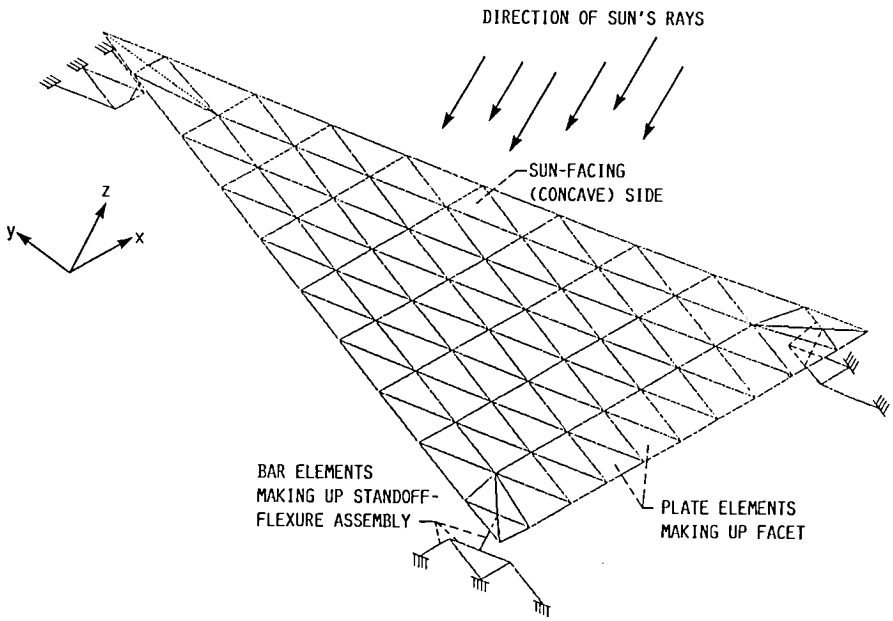

FIGURE 7. - TRIANGULAR-FACET FINITE ELEMENT MODEL.

(1) Thermal loading on the standoffs affected facet rigid-body rotation and therefore must be considered in the concentrator analysis.

(2) The through-thickness temperature gradient on the facet caused an out-of-plane displacement of the center of the facet equal to 0.025 cm (0.01 in.) relative to the corners. This resulted in an increase in the radius of curvature of 58.4, 76.1, 96.4, and 116.8 cm (23, 30, 38, and 46 in.) for each of the four facet radii (1921, 2181, 2441, and 2702 cm, respectively). Since a change in facet radius of curvature is equivalent to a change in facet focal length, temperature gradients on the facets will have a direct effect on concentrator optical performance. Therefore, temperature gradients through the facet must be accounted for in the concentrator analysis.

(3) Stiffening effects associated with curvature were small and can be neglected. Therefore, the facets in the concentrator finite element model can be modeled with "flat plate" finite elements.

(4) Nodal displacements predicted with the coarse 10-element mesh corresponded closely with those predicted with the fine 105-element mesh. Therefore, coarse structural modeling of the facet is adequate, and a coarse mesh can be used to model the facets in the concentrator model.

Hexpanel model.—The hexpanel finite element model is shown in figure 8. The model comprised hexpanel frame box beams, 24 facets with associated standoff-flexure assemblies, and two striker assemblies at each hexpanel corner. The model's complexity reflected the degree of uncertainty in the structural behavior of the hexpanel. The model was used to study the effects of uniform temperature rise and differential temperature through the hexpanel.

The hexpanel was restrained at the 12 striker ball locations in the out-of-plane direction only. The hexpanel frame box beams were modeled with QUAD4 plate elements so that the effect of differential temperature through the hexpanel from the "hot side" to the "cold side" could be accurately predicted. Also, modeling the frame beams with plate elements (rather than bar elements) gave depth to the hexpanel frame, enabling a realistic representation of the attachment of standoff-flexure assemblies and striker assemblies to the frame, as can be seen in the figure. Because facet curvature was ignored, each facet was modeled with four flat TRIA3 plate elements. The model comprised 804 nodes and 930 elements. Isotropic material behavior was assumed for all components. Two thermal load cases of importance were run:

(1) Uniform temperatures of 88 °C (190 °F) on the facets with the remaining structure at room temperature

(2) Differential temperature through the hexpanel frame: 7.2 °C (45 °F) on the Sun-facing side of the hexpanel frame box beams and 1.6 °C (35 °F) on the opposite side of the box beams, with the remaining structure at 4.4 °C (40 °F)

The results and conclusions of the substructural analysis of the hexpanel were as follows:

(1) Because the frame saw negligible movement when thermal loads were applied only to the facets, the standoff-flexure assemblies are effective in isolating the facets from the hexpanel frame. The reason for this desired behavior is the relative flexibility of the standoff-flexure assembly with respect to the hexpanel frame. Therefore, it is possible to greatly simplify the modeling details required to represent the standoff-flexure assembly in the concentrator finite element model. It is also possible now to accept the increases in facet radius of curvature due to thermal gradients predicted by the facet substructural model as being indicative of and applicable to all the facets in the concentrator. As a result, temperature gradients on the facets will not be revisited in the concentrator

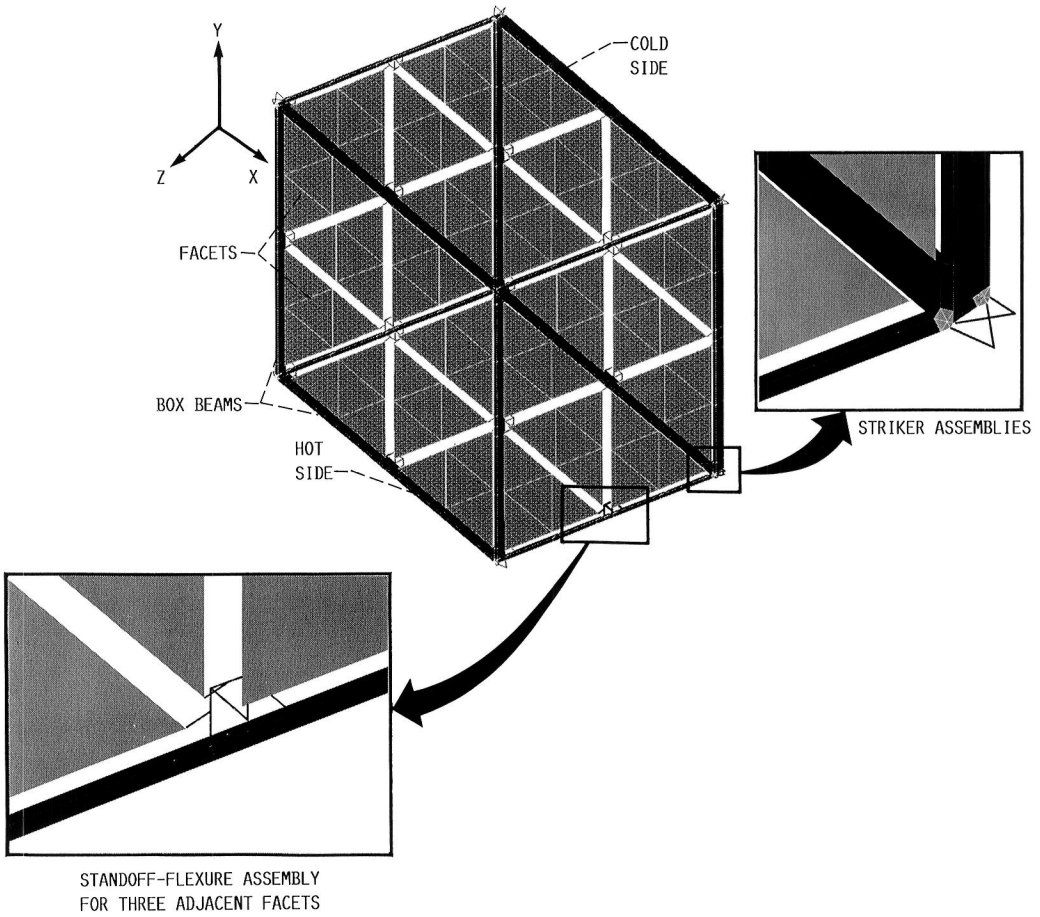

FIGURE 8. - HEXPANEL FINITE ELEMENT MODEL.

finite element analysis, but the known increases in facet radii of curvature due to thermal gradients will be accounted for directly in the NASA Lewis in-house programs that predict thermal distortion effects.

(2) Differential temperature through the depth of the hexpanel frame box beams caused large out-of-plane displacements to the hexpanel, indicating that temperature differentials (or gradients) through the hexpanel frame should be considered in the concentrator analysis. Because bar elements can model temperature differentials across both the depth and the width, they can be used to model the hexpanel frame box beams in the concentrator finite element model.

The conclusions drawn from the substructural analysis enabled the finite element representation of the concentrator to be simplified. The modeling of the concentrator based on the findings from the substructural analyses is discussed in the next section.

Concentrator Finite Element Modeling

The finite element model of the solar concentrator was created by using PATRAN. All modeling information was stored in a PATRAN data base that could be updated and revised as required before being translated to NASTRAN bulk data form.

A single hexpanel was remodeled with simplifications based on the findings from the substructural analyses. The remodeled hexpanel appears in figure 9. The hexpanel contains 223 grid points, 204 bar elements, and 72 triangular plate elements. Each hexpanel frame box beam was modeled by using four equal-length bar elements attached end to end. The bar elements were connected in all six degrees of freedom at the hexpanel corner and center node points. Four bar elements per box beam was fine enough modeling fidelity to allow accurate attachment of standoff-flexure assemblies at the corners and midsections of the frame, because of the simplified representation of the standoff-flexure assemblies in the concentrator model.

Each standoff-flexure assembly now became represented by a flexible bar element, which, in order to have its proper location with respect to the hexpanel frame maintained, was attached to the hexpanel frame corner or midsection by a rigid bar element. (This geometry can be seen in the blowup view in figure 9, which shows one continuous box beam, six rigid bar elements, and five flexible bar elements (the sixth is hidden) having unique local coordinate systems.) The flexible bar element was given a stiffness equivalent to that of the entire physical standoff-flexure assembly. The derivation of this equivalent stiffness is shown in the appendix.

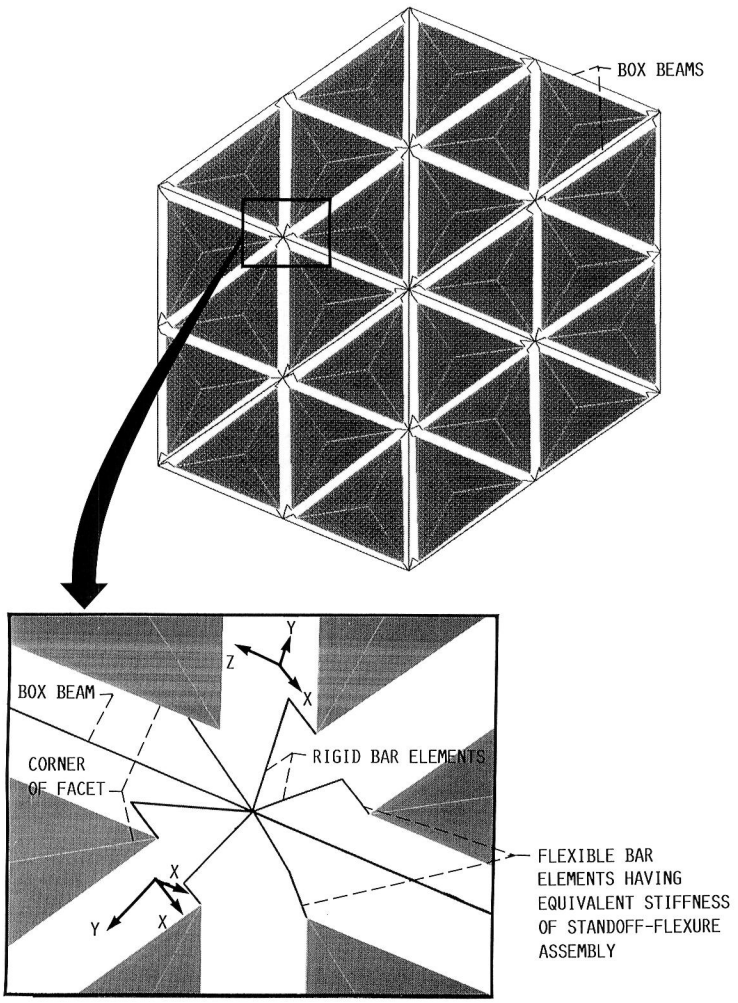

FIGURE 9. - CONCENTRATOR FINITE ELEMENT MODEL - SINGLE HEXPANEL.

The facets were modeled coarsely and without curvature by using flat triangular plate elements. Three plate elements represented each facet, enabling a node to be located at the facet center to give a more direct readout of facet rotations and translations. In the actual design a standoff is attached to the facet approximately 7.0 cm (2.75 in.) from the facet corner. So that the standoffs could be connected at the facet corners in the concentrator finite element model, the actual facet corners were shifted toward the center of the facet to the approximate standoff-facet connection point. Consequently, the facet corners were located only approximately in the finite element model and had to be later modified with the actual locations for postprocessing by the NASA Lewis in-house programs.

The concentrator model was constructed by using PATRAN commands to reproduce this hexpanel at 19 separate locations. The 19 panels had to be interconnected to form a single structure. The panels were interconnected by adding latch and striker details at the proper locations. Figure 10 shows the concentrator finite element model including the latch and striker modeling details. Each latch-striker assembly was modeled by using four flexible bar elements and four rigid bar elements. The junction point between the latch and the striker, being a ball joint, was represented by releasing the rotational degrees of freedom at the four bar ends connected at the junction grid point. The rigid bar elements were necessary to provide offsets between the panel corner grid point and the latch-striker bar ends because the hexpanel frame, being of bar element representation, was without cross-sectional depth.

The concentrator is supported by nine tubular struts. Three struts are used to provide in-plane rigidity for the concentrator; the remaining six struts are used to attach the concentrator to Space Station *Freedom* at the solar receiver. Bar elements were used to model the tubular struts. The junctures of the struts and the concentrator are pinned connections. The three nodes at the solar receiver interface are fixed in all six directions.

The PATRAN modeling of the concentrator was then completed by adding the material property cards and the bar element property cards (tables I and II). The material and the optical performance requirements of the concentrator

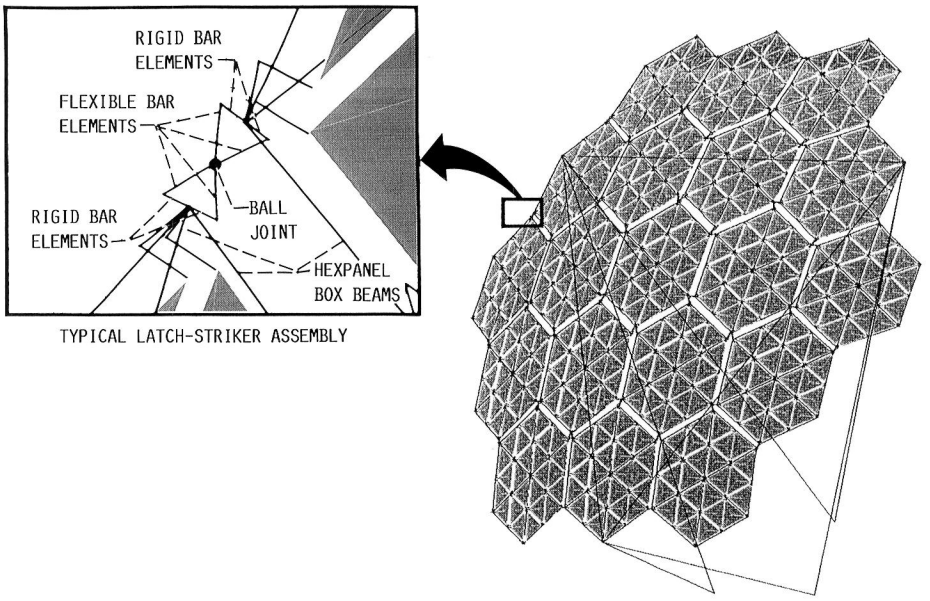

FIGURE 10. - CONCENTRATOR FINITE ELEMENT MODEL INCLUDING LATCH-STRIKER DETAILS.

TABLE I.—MATERIAL PROPERTIES

Material location	Modulus of elasticity, MPa	Poisson's ratio	Coefficient of thermal expansion, cm/cm °C
Aluminum standoff-flexures and latch-strikers	6.895×10^{4}	0.25	3.600×10^{-6}
Composite hexpanel box beams	1.793×10^{5}	.30	$-.900\times10^{-6}$
Honeycomb facets	3.650×10^{3}	.30	3.600×10^{-6}
Graphite tubular struts	2.275×10^{5}	.30	$.018\times10^{-6}$

TABLE II.—BAR ELEMENT PROPERTIES

Component	Cross-sectional area, cm^2	Moment of inertia, I_y, cm^4	Moment of inertia, I_z, cm^4	Torsional constant, cm^4
Hexpanel box beam	2.6128	40.4519	3.1150	9.6803
Standoff-flexure	.1826	2.418×10^{-3}	5.2×10^{-5}	----------
Latch-striker	1.9613	8.7409	.4162	1.4152×10^{2}
Tubular strut	9.5768	76.807	76.807	1.5359×10^{2}

demanded a more effective characterization of the effects of thermal distortion than could be inferred directly from the PATRAN nodal displacements. The additional finite element load case preparation tasks, as well as the need to predict and display the effects of ''thermally induced slope error'' on concentrator optical performance were undertaken and addressed by the NASA Lewis in-house computer programs. These in-house computer programs are described in the following section.

Analytical Procedure

Four in-house computer programs were used to perform finite element load-case preparation tasks as well as to evaluate results from the finite element analysis. These four computer programs were PANEL, SNIP (ref. 6), CONRMS, and OFFSET (ref. 7). PANEL and SNIP were used to complete the preparations for the finite element load case: PANEL revised the locations of the facet corners within the concentrator model to accurately reflect the Harris design coordinates; SNIP mapped temperature results defined under a parallel thermal analysis effort (ref. 8) to the finite element model. CONRMS and OFFSET were used to evaluate results from the finite element analysis: CONRMS made an approximate optical error calculation for each facet; OFFSET performed a ray-tracing analysis to predict actual changes in flux distribution at the solar receiver due to the thermally distorted concentrator geometry. Figure 11 shows a flow chart of the entire analytical procedure, with the program name displayed in bold, the input and output of each program shown, and the in-house programs marked with an asterisk. The following subsections describe these in-house computer programs in further detail.

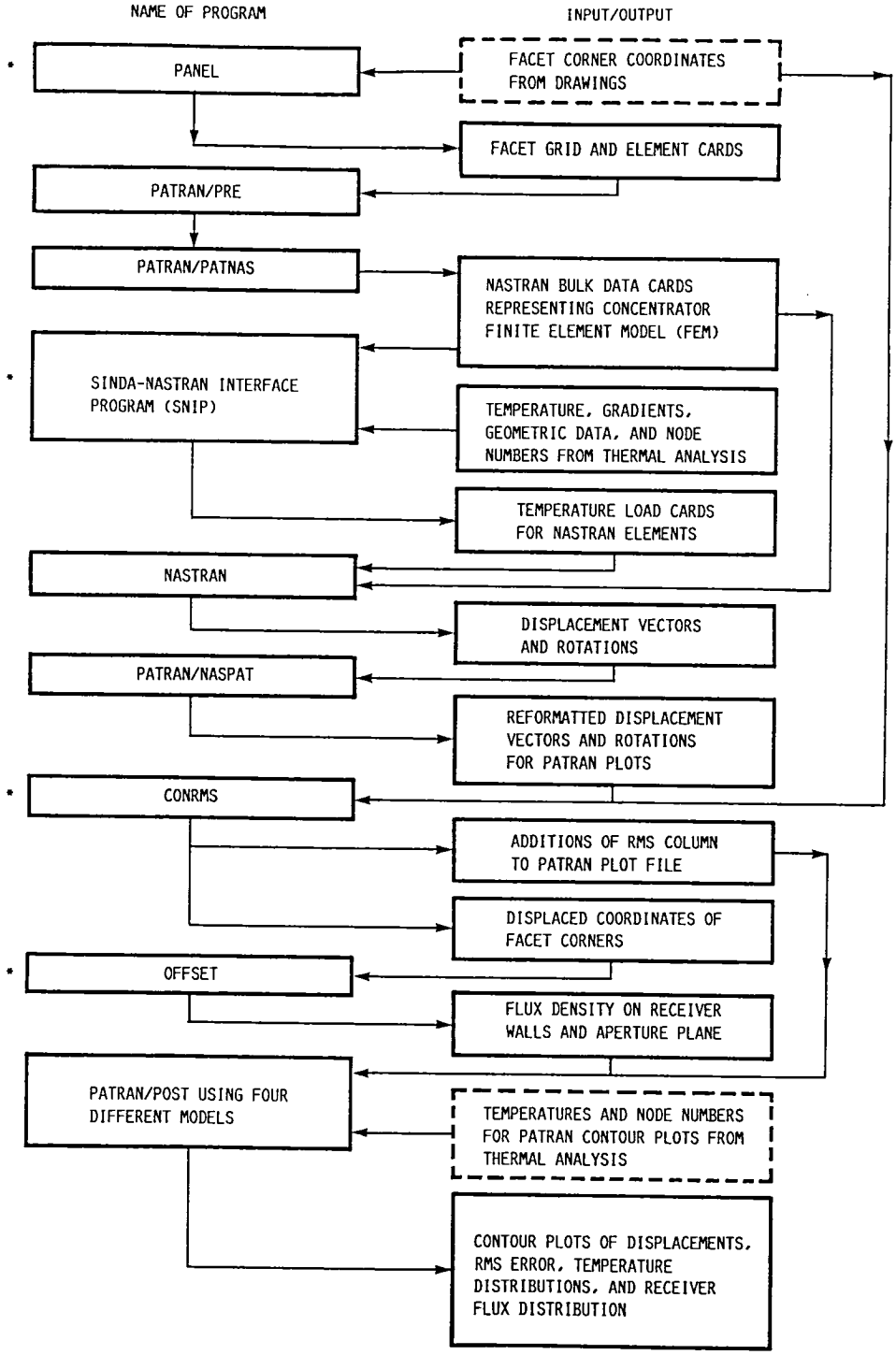

FIGURE 11. - CONCENTRATOR THERMAL DISTORTION ANALYSIS PROCEDURE. (ASTERISK DENOTES PROGRAMS DEVELOPED AT LEWIS RESEARCH CENTER.)

PANEL.—The corner locations of the facets in the finite element model were updated by using the Fortran program PANEL. PANEL accepts facet x, y, and z corner coordinates from the Harris drawings and produces new NASTRAN connectivity cards for the facets. This file of connectivity cards is then translated into neutral file format and merged with the original PATRAN data base containing the concentrator model. This merging procedure causes the original facet node and element information to be overwritten with new facet node and element information and the corner locations of all 456 facets to be revised to correctly reflect the Harris design coordinates.

PANEL was necessary because the concentrator modeling process, being based on the reproduction of a generic hexpanel, had created facets having corner locations that were only approximate in the depth direction within the hexpanel frame. Having accurate facet corner locations in the finite element model was important for two reasons. First, accurate location of the facet corners imposes a precise length to each standoff (flexible bar element) in the finite element model. A precise representation of standoff physical length was necessary because substructural analysis had indicated that thermal loading on the standoffs must be considered in the concentrator analysis. Second, the OFFSET code required displaced facet corner locations in order to predict flux profiles for distorted concentrator geometry. The process of obtaining displaced facet corner locations is simplified by initially having accurate facet corner locations in the finite element model.

SNIP.—The SINDA to NASTRAN Interface Program (SNIP) was used to eliminate the labor-intensive task of relating 798 specific thermal nodes of a parallel thermal analysis to the 4400 specific NASTRAN structural elements of the concentrator model. The thermal analysis had been performed by using the Thermal Radiation Analysis System (TRASYS) (ref. 9) and the System Improved Numerical Differencing Analyzer (SINDA) (ref. 10). SNIP is a Fortran computer program that generates NASTRAN thermal load cards for NASTRAN plate, shell, bar, and beam elements. Inputs to the SNIP program are SINDA (or similar thermal analyzer) nodal temperature results, their corresponding nodal coordinates, and the NASTRAN structural model in bulk data file form. SNIP uses a geometric search routine and a numerical coding scheme to relate thermal model nodes to structural elements. SNIP then calculates element temperatures on the basis of the weighted average of thermal node temperatures related to each element. User-controlled input parameters provide control over node-to-element correlation.

The concentrator was assumed to be in a 250-n mi altitude circular orbit, which has a period of 93.7 min with 35.7 and 58.0 min of eclipse and sunlight, respectively. The TRASYS and SINDA programs were used to predict the temperatures of the concentrator at moments in time during this orbit. Three load cases were considered in the structural analysis, corresponding to three points in time during orbit: 6, 30, and 54 min into the sunlit portion of the orbit (approximately morning, noon, and dusk). For each load case the input to the SNIP program consisted of 798 node data cards, representing 24 facets, 12 box beams, and 6 corner fitting assemblies for each of the 19 hexpanels. Associated with each node was a temperature and the centroidal x, y, and z coordinates for the component (facet, box beam, or corner fitting assembly) it represented. The node data cards representing the box beam cards contained a temperature equal to the average temperatures of the four sides of the box beam and temperature gradients in both the beam depth and width directions based on the temperature differences between top and bottom and left and right box beam sides. Each box beam had a local coordinate system in order to achieve the correct orientation of the temperature gradients within the structural element.

Certain types of thermal loading were identified from substructural analysis as being important to consider in the concentrator structural analysis: temperatures for the facets, the box beams, and the standoffs; and temperature gradients for the facets and the box beams. After user selection of the appropriate qualification and numerical coding parameters that relate the thermal and structural models, SNIP generated NASTRAN element thermal load cards for the facets, the box beams, and the standoffs for each load case. For each standoff bar element SNIP produced a weighted average temperature based on the available temperatures of the nearest facet and hexpanel corner fitting assembly. For each box beam SNIP identified with each of the four bar elements making up that box beam a temperature and both a depthwise and a widthwise temperature gradient. For each facet SNIP related a uniform temperature to all three plate elements making up the facet. Temperature gradients on the facets were accounted for directly in the ray-tracing analysis.

CONRMS.—A Fortran program called CONRMS was written to produce root-mean-square (rms) values of the rotation vector for all 456 facets. This rms rotation, an approximate optical error calculation, was required because the NASTRAN output displacement vector is useful only for describing gross concentrator deflection and does not give any sure indication of individual facet misalignment due to thermal distortion.

For each facet CONRMS calculates an rms rotation by squaring the NASTRAN displacement vector rotations about the x and y axes (the bending rotations) at all four nodes of the facet, summing these values, taking the square root of the sum, and dividing the sum by four. These rms rotations are written on the sixth column of the NASTRAN displacement vector for the respective grid points. These rms rotations are then able to be displayed graphically with PATRAN alongside the nodal displacements, as a more sophisticated indicator of optical performance degradation due to thermal distortion. In like manner, CONRMS calculates rms rotations for each panel and for the entire concentrator for all three load cases.

CONRMS also calculates the displaced facet corner locations, needed as input into the OFFSET ray-tracing program. Displaced locations are calculated by adding the x, y, and z deflections of the facet corner grid points to the actual coordinates of each of the 456 facets as supplied on the Harris drawings.

OFFSET.—A ray-tracing computer code called OFFSET was developed at the NASA Lewis Research Center specifically to predict incident flux profiles for the offset solar collector of the Space Station *Freedom* solar dynamic electric power system. This program traces rays from 50 points on the face of the Sun to 10 points on each of the 456 collector facets and from the facets through the solar receiver aperture to the walls and back face of the receiver. The facet corner locations are the principal input to the program. If the design facet corner locations are input, the resulting solar flux distribution on the receiver surface characterizes the undeformed orientation of the facets. If displaced facet corner locations due to thermal distortion are input, the effect of concentrator thermal distortions, or thermally induced slope error, on receiver flux distribution can be determined. The OFFSET program also predicts the effect of the two other optical error sources: changes in facet radius of curvature due to thermal flattening, and statistically distributed (rms) surface slope error.

Graphical output of OFFSET results requires a PATRAN model of the receiver that uses plate elements to display the energy per unit area on each of the receiver walls. This PATRAN model appears in figure 12. The receiver is cylindrical with a small aperture centered on one end to admit reflected solar rays. It has a diameter of 1.86 m (6.10 ft) and a length of 2.99 m (9.81 ft). The cylindrical surface was divided into 80 elements in the tangential direction and 18 elements in the axial direction. The back face was divided into 80 circumferential by 6 radial elements; the front aperture plate was divided into 80 circumferential by 5 radial elements. The OFFSET code calculates the flux density for each plate element and creates the PATRAN file necessary to plot the receiver flux distribution maps for the deformed concentrator. The OFFSET code also calculates the power lost to the receiver by summing the power on the elements making up the front aperture plate.

Execution of Analysis

Once the modeling revisions of PANEL and the thermal load preparation by SNIP were completed, the three NASTRAN structural load cases to determine concentrator thermal distortion were run. Figure 13 shows the thermal loading on the concentrator facets for load case 2 at 30 min into the sunlit portion of the 250-n mi altitude orbit (noon). Although not shown here, thermal loading simultaneously existed on the hexpanel box beams and the standoffs for this (and each) load case.

Once the NASTRAN results were obtained, CONRMS was run to calculate the rms rotations and the displaced facet corner locations. OFFSET used the displaced facet corner locations to calculate the receiver flux distribution profiles. As a final step, all graphical results (temperatures, displacements, rms rotations, and receiver flux distribution profiles) were displayed on PATRAN.

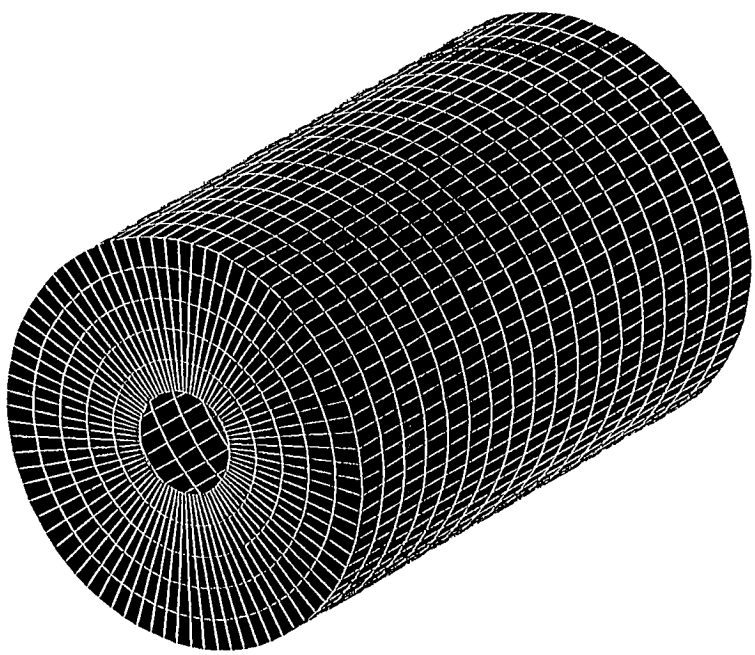

FIGURE 12. - PATRAN MODEL OF SOLAR RECEIVER.

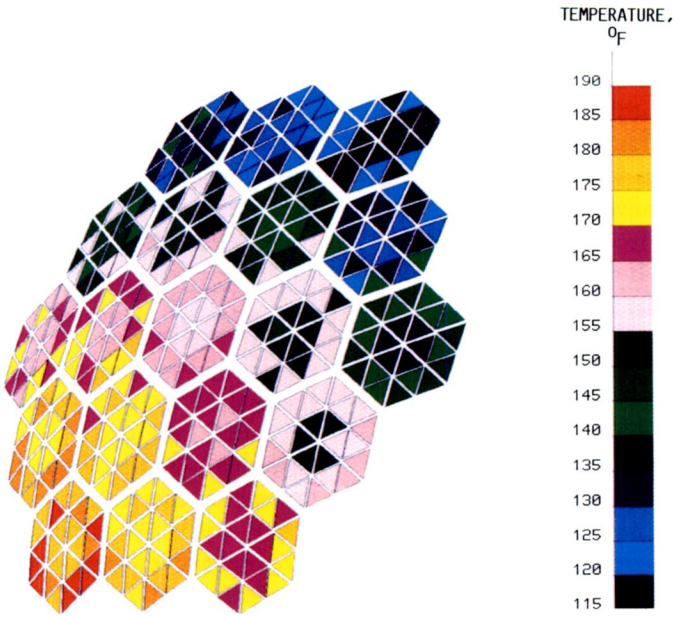

FIGURE 13. - THERMAL LOADING ON FACETS FOR LOAD CASE 2 (NOON).

Discussion of Results

A contour plot of total displacements of the concentrator facets for load case 2 is shown in figure 14. Note that total displacements varied widely across the structure. Figure 15 displays, in a head-on view of the concentrator, the facet rms rotations for the same load case. The results produced by CONRMS indicate that rms rotations for the entire concentrator are 0.04, 0.12, and 0.17 milliradian (mrad) for load case 1 (morning), load case 2 (noon), and load case 3 (dusk), respectively. Even the maximum concentrator rms rotation of 0.17 mrad is small, only about 6 percent of the 3-mrad facet slope error fabrication tolerance. This indicates from a preliminary standpoint that the effects of thermal distortion on concentrator on-orbit optical performance are small.

Results from the OFFSET ray-tracing analysis are presented in table III. This table shows the power lost to the receiver for each thermal load case as well as that lost from facet surface slope error and facet thermal flattening. It can be seen that a fabrication tolerance of 3 mrad for the facets (as is expected practically) was responsible for the greatest amount of spillage. A comparison of rms calculations and optical analysis results shows that rms calculations appear to be a good qualifying indicator of the effects of thermal distortion on concentrator performance. The combined case of 3-mrad slope error, thermal flattening of the facets, and thermal distortions actually decreased the amount of power lost from the 3-mrad error case. The reason is that the largest facet radius of curvature, 2702 cm, was actually undersized by about 200 cm (78 in.). As the facets flattened from thermal distortion, the increased radius of curvature became closer to the ideal radius of curvature. In other words, the image at the aperture was made smaller rather than larger.

Figure 16 shows the flux distribution profile on the receiver walls for the combined case. No significantly high flux rates were observed, with the maximum being 3.5 W/cm^2. The flux distribution maps were identical for all practical purposes for the three thermal load cases and the perfect facet case.

TABLE III.—POWER LOST DUE TO DIFFERENT OPTICAL ERRORS

Case description	Power lost	
	kW	Percent of total
Perfect facets (undeformed orientation)	0.4685	0.226
Facets with 3-mrad slope error	8.3713	4.042
Change in radius due to thermal flattening of facets (0.0254 cm)	.3081	.149
Thermal load case 1 (6 min into Sun)	.4515	.225
Thermal load case 2 (noon)	.4730	.228
Thermal load case 3 (3 min before eclipse)	.4770	.228
Combined thermal load case 2, thermal flattening, and 3-mrad slope error	7.9308	3.830

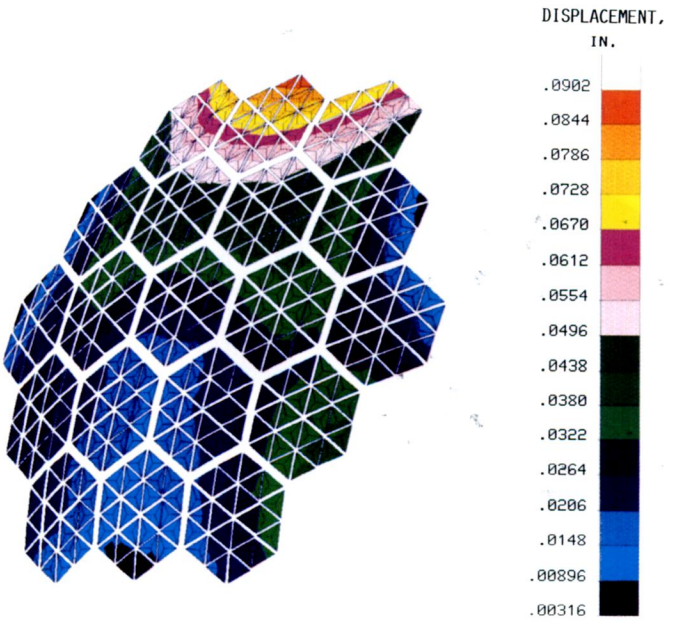

FIGURE 14. - TOTAL DISPLACEMENTS OF CONCENTRATOR FACETS FOR LOAD CASE 2.

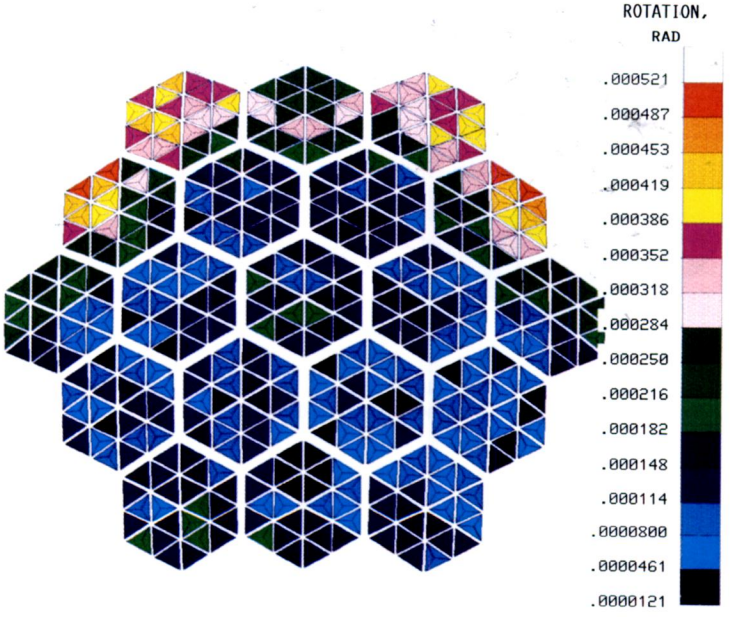

FIGURE 15. - ROOT-MEAN-SQUARE ROTATIONS OF CONCENTRATOR FACETS FOR LOAD CASE 2.

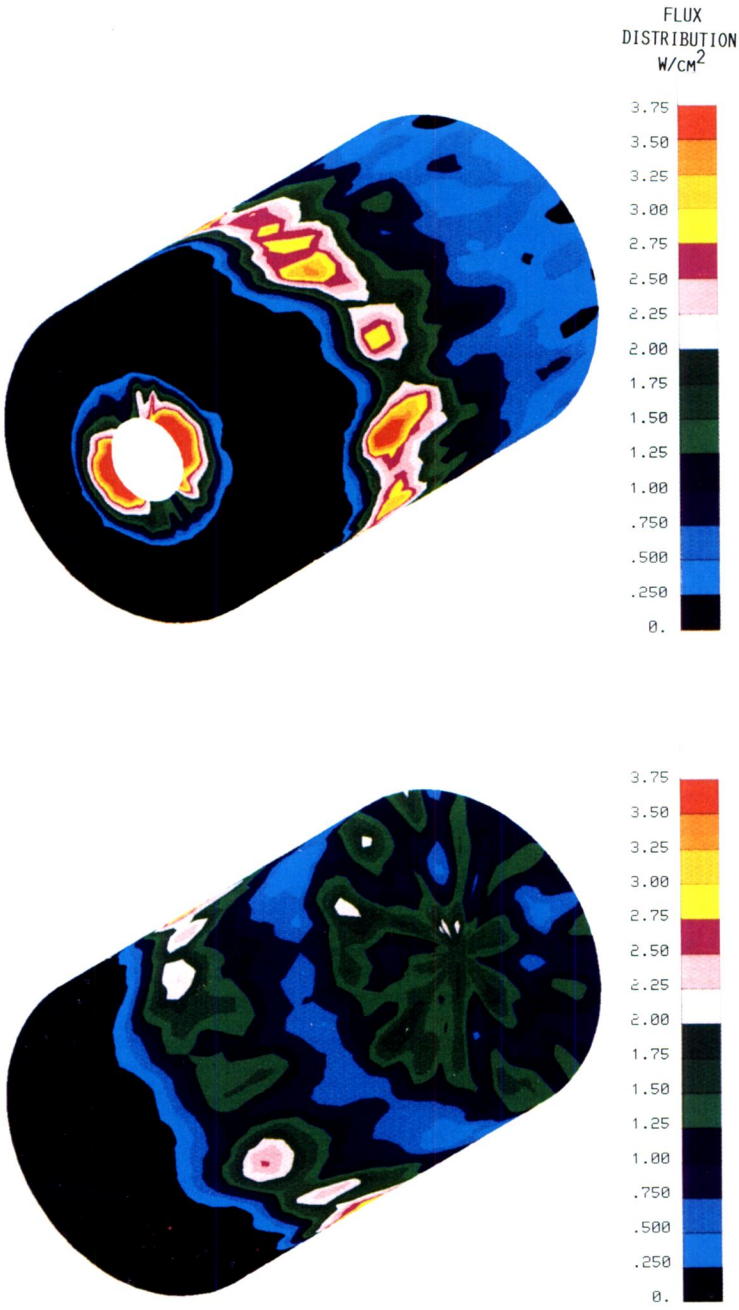

FIGURE 16. - RECEIVER FLUX DISTRIBUTION PROFILE FOR COMBINED CASE - ON-ORBIT THERMAL LOADS WITH AN INITIAL 3-MRAD FACET SLOPE ERROR.

Concluding Remarks

A finite-element-based analysis has been performed on the Space Station *Freedom* solar dynamic concentrator to predict its performance in the 250-n mi low-Earth-orbit thermal environment. A finite element structural model of the concentrator has been developed. On-orbit temperature distributions from the thermal analysis have been used for thermal loading. Specialized optical analyses, making use of the finite element displacement results, have assisted in result interpretation. The results show that the distortions of the concentrator are extremely small with respect to the size of the structure and that the effect of thermal distortions on concentrator optical performance should be negligible. In fact, the effect of on-orbit concentrator thermal distortions on solar dynamic system performance was found to be less than that caused by fabrication tolerances for optical facet hardware. This indicates the choice of materials for the solar dynamic concentrator to be excellent from the thermal design standpoint.

Appendix—Derivation of Equivalent Stiffness for Standoff-Flexure Assembly

Each standoff-flexure assembly in the concentrator finite element model is represented by a flexible bar element attached to the hexpanel frame box beam by a rigid bar element. This flexible bar element has a stiffness equivalent to that of the entire standoff-flexure assembly. The derivation of this equivalent stiffness follows.

Figure 5 shows the details and dimensions of the corner-located standoff-flexure assembly. The reference coordinate system is shown in this figure. As shown

L length of flexure bracket, 4.303 cm (1.693 in.)

T thickness of flexure bracket, 0.076 cm (0.030 in.)

W width of flexure bracket, 0.953 cm (0.375 in.)

H height of standoff, 5.080 cm (2.000 in.)

D diameter of standoff, 0.483 cm (0.190 in.).

Let

$$\text{def } y = \Delta s_y + \Delta f_y + (H\theta_{fz})$$

and

$$\text{def } z = \Delta s_z + \Delta f_z + (H\theta_{fy})$$

where

def y total deflection at standoff ball in y direction due to load P

def z total deflection at standoff ball in z direction due to load P

Δs_y deflection of standoff ball with respect to standoff base (jam nut) in y direction due to load P at standoff ball in y direction, cm

Δs_z deflection of standoff ball with respect to standoff base (jam nut) in z direction due to load P at standoff ball in z direction, cm

Δf_y deflection of flexure bracket in y direction due to load P at its midspan in y direction, cm

Δf_z deflection of flexure bracket in z direction due to load P at its midspan in z direction, cm

θ_{fy} rotation of flexure bracket about y axis, rad

θ_{fz} rotation of flexure bracket about z axis, rad

Calculation of Def y

$$\text{def } y = \Delta s_y + \Delta f_y + (H\theta_{fz})$$

From reference 11, page 96, case 1a:

$$\Delta s_y = \frac{PH^3}{3EI_{sz}} \tag{A1}$$

where

P load applied at standoff ball in y direction, N

H height of standoff, 5.080 cm

E Young's modulus for aluminum, 6.895×10^4 MPa (10.0×10^6 psi)

I_{sz} moment of inertia for standoff about z-z axis, $\pi D^4/64$, 2.6715×10^{-3} cm^4 (0.653×10^{-4} in.^{4})

Therefore,

$$\Delta s_y = 2.372\times10^{-3}\ P$$

From reference 11, page 97, case 1d:

$$\Delta f_y = \frac{PL^3}{192EI_{fx}} \tag{A2}$$

where

P load applied at flexure midspan in y direction, N

L length of flexure bracket, 4.303 cm

E Young's modulus for aluminum, 6.895×10^4 MPa

I_{fx} moment of inertia for flexure about x-x axis, $WT^3/12$, 3.49×10^{-5} cm^4 (0.838×10^{-6} in.^{4})

Therefore,

$$\Delta f_y = 1.724\times10^{-3}\ P$$

From reference 11, page 287, eq. (1):

$$\theta_{fz} = \frac{t\ell}{JG} \tag{A3}$$

where

t twisting moment, $(P/2)H$, N-cm

ℓ length of member, or half-length of flexure bracket, $L/2$, 2.152 cm (0.847 in.)

J polar moment of inertia of flexure bracket, $(W/2)(T/2)^3$ [$(16/3) - 3.36(T/W)$], 1.324×10^{-4} cm^4 (0.318×10^{-5} in.^{4})

G modulus of rigidity for aluminum, 1.793×10^4 MPa (2.6×10^6 psi)

Therefore,

$$\theta_{fz} = 2.3025\times10^{-2}\ P$$

As a result

$$\begin{aligned}\text{def } y &= \Delta s_y + \Delta f_y + (H\theta_{fz})\\ &= [2.372 + 1.724 + (5.080\times23.025)]\times10^{-3}\ P\\ &= 0.121063\ P\end{aligned}$$

Calculation of Def z

$$\text{def } z = \Delta s_z + \Delta f_z + (H\theta_{fy})$$

Since the standoff bar is of circular cross section,

$$\Delta s_z = \Delta s_y = 2.372\times10^{-3}\ P$$

The flexure bracket is assumed to have no deflection in the z direction owing to a load P at its midspan in the z direction; therefore, $\Delta f_z = 0$.

From reference 11, page 103, case 3d, the following expression can be derived:

$$\frac{ML}{16EI_{fy}} \tag{A4}$$

where

M applied couple, $PH = 5.08P$, N-cm

L length of flexure bracket, 4.303 cm

E Young's modulus for aluminum, 6.895×10^4 MPa

I_{fy} moment of inertia for flexure about y-y axis, $TW^3/12$, 5.4816×10^{-3} cm^4

Therefore,

$$\theta_{fy} = 3.6\times10^{-5}\ P$$

As a result

$$\begin{aligned}\text{def } z &= \Delta s_z + \Delta f_z + (H\theta_{fy})\\ &= [237.2 + 0.0 + (5.080\times3.6)]\times10^{-5}\ P\\ &= 0.002555\ P\end{aligned}$$

To make the flexible bar element have a stiffness equivalent to that of the entire standoff-flexure assembly, one need only calculate the principal flexural moments of inertia for a 5.080-cm-long cantilevered bar that yield the same y and z deflections (def y and def z) calculated here. From equation (A1):

$$\text{def } y = \frac{PH^3}{3EI_{zeq}}$$

where

$$H = 5.080 \text{ cm}$$

$$E = 6.895\times10^4 \text{ MPa}$$

$$\text{def } y = 0.121063\ P$$

As a result

$$I_{zeq} = \frac{P(5.080)}{3E(0.121063\ P)} = 5.2\times10^{-5} \text{ cm}^4$$

Likewise,

$$I_{yeq} = \frac{P(5.080)^3}{3E \text{ def } z}$$

where

$$E = 6.895\times10^4 \text{ MPa}$$

$$\text{def } z = 0.002555\ P$$

As a result

$$I_{yeq} = 2.481\times10^{-3} \text{ cm}^4$$

In the concentrator finite element model a local coordinate system is defined for each flexible bar element so that these principal flexural moments of inertia, I_{yeq} and I_{zeq}, are of proper orientation. In the blowup view in figure 9, local coordinate systems for two of the six flexible bar elements are shown.

References

1. Solar Concentrator Advanced Development Program, Task 1. NASA CR-179489, 1986.
2. Valade, F.H.: Space Station Solar Concentrator Development. Solar Engineering 1988, L.M. Murphy and T.R. Mancini, eds., ASME, New York, 1988, pp. 369-374.
3. Corrigan, R.D.; and Ehresman, D.T.: Solar Concentrator Advanced Development Project. Energy—New Frontiers, (22nd IECEC), Vol. 1, AIAA, New York, 1987, pp. 156-161.
4. PATRAN II User's Guide, Vols. I and II and Enhancements. PDA Engineering, Santa Ana, CA, 1985.
5. McCormack, C.W., ed.: MSC/NASTRAN User's Manual. Version 63, MacNeill Schwendler Corp., 1983.
6. Winegar, S.R.: SINDA-NASTRAN Interfacing Program Theoretical Description and User's Manual. NASA TM-100158, 1987.
7. Jefferies, K.S.: Ray Tracing Optical Analysis of Offset Solar Collector for Space Station Solar Dynamic System. NASA TM-100853, 1988.
8. Trudell, J.J.; Dalsania, V.; Baumeister, J.F.; and Jefferies, K.S.: Thermal Distortion Analysis of the Space Station Solar Dynamic Concentrator. NASA TM-100868, 1988.
9. Thermal Radiation Analysis System, TRASYS II, User's Manual. MCR-73-105, Rev. 5, Martin Marietta, 1983.
10. Smith, J.P.: SINDA User's Manual, Rev. 3, COSMIC Program MSC-13805, 1983.
11. Roark, R.J.; and Young, W.C.: *Formulas for Stress and Strain*, Fifth ed., McGraw-Hill Book Company, 1975.

NASA
National Aeronautics and Space Administration

Report Documentation Page

1. Report No.	2. Government Accession No.	3. Recipient's Catalog No.
NASA TM-102504		

4. Title and Subtitle	5. Report Date
Finite Element Analysis of Thermal Distortion Effects on Optical Performance of Solar Dynamic Concentrator for Space Station *Freedom*	July 1990
	6. Performing Organization Code

7. Author(s)	8. Performing Organization Report No.
Michael P. Doherty and Vithal Dalsania	E-5305
	10. Work Unit No. 474-12-10

9. Performing Organization Name and Address	11. Contract or Grant No.
National Aeronautics and Space Administration Lewis Research Center Cleveland, Ohio 44135-3191	
	13. Type of Report and Period Covered Technical Memorandum

12. Sponsoring Agency Name and Address	14. Sponsoring Agency Code
National Aeronautics and Space Administration Washington, D.C. 20546-0001	

15. Supplementary Notes

16. Abstract

An analysis has been performed to predict the thermal distortion of the solar dynamic concentrator for Space Station *Freedom* in low Earth orbit and to evaluate the effects of that thermal distortion on concentrator on-orbit performance. The analysis required substructural finite element modeling of critical concentrator structural subsystems, structural finite element modeling of the concentrator, mapping of thermal loading onto the structural finite element model, and the creation of specialized postprocessors to assist in interpreting results. Concentrator temperature distributions and thermally induced displacements and slope errors and the resulting receiver flux distribution profiles are discussed. Results determined for a typical orbit indicate that concentrator facet rotations are less than 0.2 mrad and that the change in facet radius due to thermal flattening is less than 5 percent. The predicted power loss due to thermal distortion effects is less than 0.3 percent. As a consequence the thermal distortions of the solar dynamic concentrator in low Earth orbit will have a negligible effect on the flux distribution profiles within the receiver.

17. Key Words (Suggested by Author(s))	18. Distribution Statement
Space station; Electrical power system; Solar dynamic concentrator; Thermal loads; Optical performance	Unclassified – Unlimited Subject Category 37

19. Security Classif. (of this report)	20. Security Classif. (of this page)	21. No. of pages	22. Price*
Unclassified	Unclassified	20	A03

*For sale by the National Technical Information Service, Springfield, Virginia 22161

National Aeronautics and
Space Administration

Lewis Research Center
Cleveland, Ohio 44135

NASA

DO NOT REMOVE SLIP FROM MATERIAL

Delete your name from this slip when returning material to the library.

NAME	DATE	MS
P. Howell	6/94	231

NASA Langley (Rev. Dec. 1991) RIAD N-75